applied sciences

MDPI

Article

Bulk and Rayleigh Waves Propagation in Three-Phase Soil with Flow-Independent Viscosity

Qing Guo [1,2], Hongbo Liu [1,2], Guoliang Dai [1,2,*] and Zhongwei Li [1,2]

[1] School of Civil Engineering, Southeast University, Nanjing 210096, China; guoqingah@163.com (Q.G.); lhb_0803@163.com (H.L.); lizw@seu.edu.cn (Z.L.)
[2] Key Laboratory of Concrete and Prestressed Concrete Structure of Ministry of Education, Southeast University, Nanjing 210096, China
* Correspondence: daigl@seu.edu.cn

Abstract: The flow-independent viscosity of the soil skeleton has significant influence on the elastic wave propagation in soils. This work studied the bulk and Rayleigh waves propagation in three-phase viscoelastic soil by considering the contribution of the flow-independent viscosity from the soil skeleton. Firstly, the viscoelastic dynamic equations of three-phase unsaturated soil are developed with theoretical derivation. Secondly, the explicit characteristic equations of bulk and Rayleigh waves in three-phase viscoelastic soil are yielded theoretically by implementing Helmholtz resolution for the displacement vectors. Finally, the variations of the motion behavior for bulk and Rayleigh waves with physical parameters such as relaxation time, saturation, frequency, and intrinsic permeability are discussed by utilizing calculation examples and parametric analysis. The results reveal that the influence of soil flow-independent viscosity on the wave speed and attenuation coefficient of bulk and Rayleigh waves is significantly related to physical parameters such as saturation, intrinsic permeability, and frequency.

Keywords: bulk wave; Rayleigh wave; viscoelasticity; unsaturated soil; wave speed; attenuation coefficient

Citation: Guo, Q.; Liu, H.; Dai, G.; Li, Z. Bulk and Rayleigh Waves Propagation in Three-Phase Soil with Flow-Independent Viscosity. *Appl. Sci.* **2022**, *12*, 7166. https://doi.org/10.3390/app12147166

Academic Editors: Fabio Di Pietrantonio

Received: 10 June 2022
Accepted: 13 July 2022
Published: 16 July 2022

Publisher's Note: MDPI stays neutral with regard to jurisdictional claims in published maps and institutional affiliations.

Copyright: © 2022 by the authors. Licensee MDPI, Basel, Switzerland. This article is an open access article distributed under the terms and conditions of the Creative Commons Attribution (CC BY) license (https://creativecommons.org/licenses/by/4.0/).

1. Introduction

The wave motion behavior in natural earth foundation is a fundamental scientific problem for theoretical study (e.g., soil dynamics) and practical engineering (e.g., nondestructive examination of natural and artificial materials in foundation soil). Generally, bulk and surface waves are captured in the natural earth foundation. Bulk waves, including longitudinal and transverse waves, are the seismic waves generated by source vibrations and are propagated in the media. Surface waves, such as Rayleigh waves, are secondary waves derived from bulk waves on the surface or layered surface of media. On the other side, the natural earth foundation can be divided into entirely and partially saturated states. The wave propagation behavior in partially saturated soil is significantly more complex than that in completely saturated soil because the capillary pressure and coupling effect will affect the motion behaviors of elastic waves in unsaturated soil [1,2].

Undoubtedly, the emergence of Biot theory [3,4] and mixture theory [5] not only give the sound basis for the research of wave theory but accelerate the research process. For the bulk and Rayleigh waves propagation in saturated soil, researchers including Jones [6], Plona [7], Berryman [1], Berryman [8,9], Zhou and Ma [10], Straughan et al. [11], Rohan et al. [12], Tung [13], and Wang et al. [14] implemented several theoretical and experimental works. They drew that the longitudinal, transverse, and Rayleigh waves depend on not only the frequency but the soil parameters such as permeability and soil mass types. Additionally, the applied research on the dynamic response of natural foundation also aroused broad concern from researchers [15–18], which undoubtedly promotes the

basic research on wave propagation in completely saturated soils. In recent years, with the improvement of mathematics solving ability and engineering precision requirements, several researchers, including Lo [19], Lo et al. [20], and Liu et al. [21–23], have implemented works on the bulk and Rayleigh waves propagation in three-phase partially saturated soil. These works concluded that a kind of longitudinal wave (typically named P_3 wave) exists in three-phase soil, and the liquid saturation has a significant effect on the bulk and Rayleigh waves.

Additionally, it is usually recognized that the deformation of the soil, even dry soil, is related to time. That is, the soil viscosity is dependent on the soil skeleton viscosity. Nonetheless, most of the existing works on wave propagation in unsaturated soils only take into account the fluid viscosity but seldom mention the effect of solid skeleton viscosity. Appreciatively, the relationship between soil-structure response and the soil skeleton viscosity has been proposed by researchers [24,25]. Moreover, recently, the dependence of soil skeleton viscosity on the motion behaviors of elastic waves in saturated soils has been studied with an analytical solution [26]. To overcome the lack of previous research on the relationship between the soil skeleton viscosity (flow-independent viscosity) and the elastic wave propagation in unsaturated soil, this work simplifies the unsaturated saturated soils to the multiphase mixture consisting of soil particles, water, and air. The viscoelastic wave equations are established with the Biot model, mixture theory, and the generalized Kelvin–Voigt model. Then, the characteristic formulas of longitudinal, transverse, and Rayleigh waves are yielded with theoretical derivation. Finally, the relationships between the motion behaviors (speed and attenuation) of each wave and the soil parameters are graphed and discussed by utilizing calculation examples and parametric analysis.

2. Viscoelastic Dynamic Model

Generally, the deformation of viscoelastic materials is strictly associated with the loading force and relaxation time of stress and strain. Usually, the damping of three-phase unsaturated soil to the elastic wave propagation mainly comes from two aspects: owne is the viscosity from the solid skeleton, called flow-independent viscosity, and the other is the viscosity from the liquid and gas in pores, called flow-dependent viscosity. To express the flow-independent viscosity in three-phase unsaturated soil, the generalized Kelvin–Voigt model [27,28] is introduced in this study, as illustrated in Figure 1. The dashpot depicted in Figure 1 is utilized to represent the negative effect of the solid skeleton on elastic wave propagation.

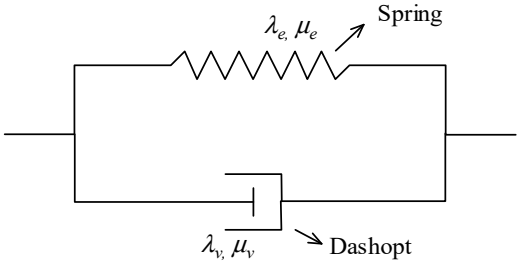

Figure 1. Generalized Kelvin–Voigt model [27,28].

In Figure 1, the spring represents the linear-elastic response of the solid skeleton in unsaturated soil under load, while the dashpot represents the damping behaviors of the solid skeleton in unsaturated soil. The dashpot avoids the spring directly reaching the load. The correlation between elastic constants and viscous constants of viscoelastic soils can be expressed as [29]

$$\lambda_v = t_s \lambda_e, \ \mu_v = t_s \mu_e \tag{1}$$

where the two sets of symbols λ_e, μ_e and λ_v, μ_v stand for the elastic and viscosity constants of soil, respectively. t_s stands for the relaxation time, representing the normalized viscosity without loss of generality [24,30]. In this article, t_s is utilized to evaluate the viscosity of the solid skeleton, that is, the magnitude of flow-independent viscosity.

In this work, the unsaturated soil is assumed to be homogeneous, isotropic, and viscoelastic material with multiple pores, composed of liquid and gas occupying pores as well as solid particles. The liquid (water) saturation and gas (air) saturation are represented by S^r and S^a, respectively, and the constraint $S^r + S^a = 1$ is satisfied in this work.

According to Biot porous medium theory, the motion equation of the partially saturated soil, when ignoring the body forces and dissipation, can be expressed as [31]

$$\sigma_{ij,j} = \overline{\rho}^s \ddot{u}_i^s + \overline{\rho}^l \ddot{u}_i^l + \overline{\rho}^a \ddot{u}_i^a \tag{2}$$

where $\overline{\rho}^s = (1 - n^s)\rho^s$, $\overline{\rho}^l = n^s S^r \rho^l$, and $\overline{\rho}^a = n^s S^a \rho^a$. The nomenclature of all the Roman and Greek symbols is stated in Nomenclature. To save space, the nomenclature (physical meaning) of the symbols in the formulas used below is listed in Nomenclature, and this point will not be repeated.

According to Bishop and Blight [32], the following formula is yielded

$$\sigma'_{ij} = \sigma_{ij} + p\delta_{ij} \tag{3}$$

where $p = S^r p_l + (1 - S^r)p_a$ represents the pore fluid pressure formed by liquid and gas in pores.

The stress–strain relationship of the solid skeleton is described as [33]

$$\sigma'_{ij} = c^s_{ij}\varepsilon_{ij} - c^e_{ij}\varepsilon^p_{ij} \tag{4}$$

The strain tensors under the general state and the pore pressure are written, respectively, as [33]

$$\varepsilon_{ij} = \frac{1}{2}\left(u^s_{i.j} + u^s_{j.i}\right) \tag{5}$$

$$\varepsilon^p_{11} = \varepsilon^p_{22} = \varepsilon^p_{33} = -\frac{1}{3K_s}p \tag{6}$$

The effective stress tensor of unsaturated soil is yielded through combining Equations (4)–(6), as

$$\sigma'_{ij} = \left(\lambda_e\varepsilon_v + \lambda_v\frac{\partial\varepsilon_v}{\partial t}\right)\delta_{ij} + 2\left(\mu_e\varepsilon_{ij} + \mu_v\frac{\partial\varepsilon_{ij}}{\partial t}\right) + \frac{K_b}{K_s}p\delta_{ij} \tag{7}$$

where $\varepsilon_v = u^s_{i,i}$, and $K_b = \lambda_e + 2\mu_e/3$.

The total stress of unsaturated soil is yielded by substituting Equation (7) into Equation (3), as

$$\sigma_{ij} = \left(\lambda_e\varepsilon_v + \lambda_v\frac{\partial\varepsilon_v}{\partial t}\right)\delta_{ij} + 2\left(\mu_e\varepsilon_{ij} + \mu_v\frac{\partial\varepsilon_{ij}}{\partial t}\right) - \alpha_e p\delta_{ij} \tag{8}$$

where $\alpha_e = 1 - K_b/K_s$.

The stress component acting on the soil skeleton, denoted by σ^s_{ij}, can be assumed to

$$\sigma^s_{ij} = \frac{1}{1-n^s}\left[\sigma_{ij} + n^s S^r p_l\delta_{ij} + n^s\left(1 - S^r\right)p_a\delta_{ij}\right] \tag{9}$$

Substituting Equation (8) into Equation (9) and making algebraic operations, Equation (9) can be re-expressed as

$$\sigma_{ij}^{s}=\frac{1}{1-n^{s}}\left[\left(\lambda_{e}\varepsilon_{v}+\lambda_{v}\frac{\partial\varepsilon_{v}}{\partial t}\right)\delta_{ij}+2\left(\mu_{e}+\mu_{v}\frac{\partial}{\partial t}\right)\varepsilon_{ij}+\left(n^{s}-\alpha_{e}\right)\left[S^{r}p_{l}+\left(1-S^{r}\right)p_{a}\right]\delta_{ij}\right] \tag{10}$$

The mass balance equation of each phase is constructed after ignoring phase transitions between components, as

$$\partial\overline{\rho}^{b}/\partial t+\left(\overline{\rho}^{b}\dot{u}_{i}^{b}\right)_{,i}=0\quad b=s,l,a \tag{11}$$

Further expansion of Equation (11) yields the following formulas as

$$-\dot{n}^{s}+\left(1-n^{s}\right)\frac{\dot{\rho}^{s}}{\rho^{s}}+\left(1-n^{s}\right)\dot{u}_{i,i}^{s}=0 \tag{12}$$

$$n^{s}\dot{S}^{r}+\dot{n}^{s}S^{r}+n^{s}S^{r}\frac{\dot{\rho}^{l}}{\rho^{l}}+n^{s}S^{r}\dot{u}_{i,i}^{l}=0 \tag{13}$$

$$-n^{s}\dot{S}^{r}+\dot{n}^{s}\left(1-S^{r}\right)+n^{s}\left(1-S^{r}\right)\frac{\dot{\rho}^{a}}{\rho^{a}}+n^{s}\left(1-S^{r}\right)\dot{u}_{i,i}^{a}=0 \tag{14}$$

Following Zhang et al. [33], the derivative of each phase density with time is written as

$$\frac{\partial\rho^{s}}{\partial t}=-\frac{\rho^{s}\dot{\sigma}_{ii}^{s}}{3K_{s}},\ \frac{\partial\rho^{l}}{\partial t}=\frac{\rho^{l}\dot{p}_{l}}{K_{l}},\ \frac{\partial\rho^{a}}{\partial t}=\frac{\rho^{a}\dot{p}_{a}}{K_{a}} \tag{15}$$

According to the relationship between matric suction and saturation of unsaturated soil, established by Van Genuchten [34], the following formula is yielded

$$\dot{S}^{r}=\chi md\left(1-S_{res}\right)S_{e}^{\frac{m+1}{m}}\left(S_{e}^{-\frac{1}{m}}-1\right)^{\frac{d-1}{d}}\left(\dot{p}_{l}-\dot{p}_{a}\right) \tag{16}$$

where $S_e = (S^r - S_{res})/(1 - S_{res})$.

Substituting the first formula in Equation (15) into Equation (12) yields the derivative of porosity over time as

$$\dot{n}^{s}=\left(\alpha_{e}-n^{s}\right)\dot{u}_{i,i}^{s}-\alpha_{v}\dot{u}_{i,i}^{s}+\frac{\alpha_{e}-n^{s}}{K_{s}}S^{r}\dot{p}_{l}+\frac{\alpha_{e}-n^{s}}{K_{s}}\left(1-S^{r}\right)\dot{p}_{a} \tag{17}$$

where $\alpha_v = (3\lambda_v + 2\mu_v) / 3K_s$.

Substituting Equations (15)–(17) into Equations (13) and (14), the following formulas are yielded

$$T_{11}p_{l}+T_{12}p_{a}+T_{13}u_{i,i}^{s}+T_{14}u_{i,i}^{l}+T_{15}u_{i,i}^{a}+T_{16}\dot{u}_{i,i}^{s}=0 \tag{18}$$

$$T_{21}p_{l}+T_{22}p_{a}+T_{23}u_{i,i}^{s}+T_{24}u_{i,i}^{l}+T_{25}u_{i,i}^{a}+T_{26}\dot{u}_{i,i}^{s}=0 \tag{19}$$

in which

$$T_{11}=n^{s}A_{s}+\left(S^{r}\right)^{2}\left(\alpha_{e}-n^{s}\right)/K_{s}+S^{r}n^{s}/K_{l},\ T_{12}=S^{r}\left(1-S^{r}\right)\left(\alpha_{e}-n^{s}\right)/K_{s}-n^{s}A_{s},$$
$$T_{13}=S^{r}\left(\alpha_{e}-n^{s}\right),\ T_{14}=S^{r}n^{s},\ T_{15}=0,\ T_{16}=-\alpha_{v}S^{r},\ T_{21}=T_{12},$$
$$T_{22}=n^{s}A_{s}+\left(\alpha_{e}-n^{s}\right)S^{a}S^{a}/K_{s}+n^{s}S^{a}/K_{a},\ T_{23}=S^{a}\left(\alpha_{e}-n^{s}\right),\ T_{24}=0,\ T_{25}=n^{s}S^{a},$$
$$T_{26}=-\alpha_{v}S^{a},\ A_{s}=\chi md\left(1-S_{res}\right)\left(S_{e}^{-1/m}-1\right)^{(d-1)/d}S_{e}^{(m+1)/m}.$$

Making some algebraic operations for Equations (18) and (19), the pore-fluid pressures are yielded as

$$-p_l = t_{11}u^s_{i,i} + t_{12}u^l_{i,i} + t_{13}u^a_{i,i} + t_{14}\ddot{u}^s_{i,i} \tag{20}$$

$$-p_a = t_{21}u^s_{i,i} + t_{22}u^l_{i,i} + t_{23}u^a_{i,i} + t_{24}\ddot{u}^s_{i,i} \tag{21}$$

in which

$$t_{11} = \frac{T_{13}T_{22} - T_{23}T_{12}}{T_{11}T_{22} - T_{21}T_{12}},\ t_{12} = \frac{T_{14}T_{22}}{T_{11}T_{22} - T_{21}T_{12}},\ t_{13} = \frac{-T_{25}T_{12}}{T_{11}T_{22} - T_{21}T_{12}},\ t_{14} = \frac{T_{16}T_{22} - T_{26}T_{12}}{T_{11}T_{22} - T_{21}T_{12}}$$

$$t_{21} = \frac{T_{13}T_{21} - T_{23}T_{11}}{T_{12}T_{21} - T_{22}T_{11}},\ t_{22} = \frac{T_{14}T_{21}}{T_{12}T_{21} - T_{22}T_{11}},\ t_{23} = \frac{-T_{25}T_{11}}{T_{12}T_{21} - T_{22}T_{11}},\ t_{24} = \frac{T_{16}T_{21} - T_{26}T_{11}}{T_{12}T_{21} - T_{22}T_{11}}.$$

The motion formulas of fluid phases accounting for the effect of pore tortuosity are formulated as [33,35]

$$-p_{l,i} = \frac{\mu_l}{k^l_r k} n^s S^r \left(\dot{u}^l_i - \dot{u}^s_i\right) + \rho^l \ddot{u}^l_i + (\tau_l - 1)\rho^l \left(\ddot{u}^l_i - \ddot{u}^s_i\right) \tag{22}$$

$$-p_{a,i} = \frac{\mu_a}{k^a_r k} n^s S^a \left(\dot{u}^a_i - \dot{u}^s_i\right) + \rho^a \ddot{u}^a_i + (\tau_a - 1)\rho^a \left(\ddot{u}^a_i - \ddot{u}^s_i\right) \tag{23}$$

According to the model established by Mualem [36], the relative permeabilities k^l_r and k^g_r are written as

$$k^l_r = (S_e)^{0.5}\left[1 - \left(1 - (S_e)^{1/m}\right)^m\right]^2,\ k^a_r = (1 - S_e)^{0.5}\left[\left(1 - (S_e)^{1/m}\right)^m\right]^2 \tag{24}$$

Combination of Equations (20)–(23) and introduction of the relative displacement of liquid ($u^w_i = n^s S^r(u^l_i - u^s_i)$) and gas ($u^g_i = n^s S^a(u^a_i - u^s_i)$) phases yield the following formulas

$$\mu_e u^s_{i,jj} + (C_{11} + \mu_e)u^s_{j,ji} + C_{12}u^w_{j,ji} + C_{13}u^g_{j,ji} + \mu_v \dot{u}^s_{i,jj} + (C_{14} + \mu_v)\dot{u}^s_{j,ji} = \rho \ddot{u}^s_i + \rho^l \ddot{u}^w_i + \rho^a \ddot{u}^g_i \tag{25}$$

$$C_{21}u^s_{j,ji} + C_{22}u^w_{j,ji} + C_{23}u^g_{j,ji} + C_{24}\dot{u}^s_{j,ji} = \rho^l \ddot{u}^s_i + \nu_w \ddot{u}^w_i + b_w \dot{u}^w_i \tag{26}$$

$$C_{31}u^s_{j,ji} + C_{32}u^w_{j,ji} + C_{33}u^g_{j,ji} + C_{34}\dot{u}^s_{j,ji} = \rho^a \ddot{u}^s_i + \nu_g \ddot{u}^g_i + b_g \dot{u}^g_i \tag{27}$$

with

$$D_1 = t_{11} + t_{12} + t_{13},\ D_2 = t_{21} + t_{22} + t_{23},\ \rho = \left(1 - n^s\right)\rho^s + n^s S^r \rho^l + n^s S^a \rho^a,$$
$$C_{11} = \lambda_e + S^r \alpha_e D_1 + \left(1 - S^r\right)D_2 \alpha_e,\ C_{12} = \left[S^r t_{12} + \left(1 - S^r\right)t_{22}\right]\alpha_e \Big/ \left(n^s S^r\right),$$
$$C_{13} = \alpha_e\left(S^r t_{13} + S^a t_{23}\right)\Big/\left(n^s S^a\right),\ C_{14} = \lambda_v + \alpha_e\left(S^r t_{14} + S^a t_{24}\right),\ C_{21} = D_1,\ C_{22} = t_{12}\Big/\left(n^s S^r\right)$$
$$,\ C_{23} = t_{13}\Big/\left(n^s S^a\right),\ C_{24} = t_{14},\ C_{31} = D_2,\ C_{32} = t_{22}\Big/\left(n^s S^r\right),\ C_{33} = t_{23}\Big/\left(n^s S^a\right),$$
$$C_{34} = t_{24},\ \nu_w = \tau_l \rho^l \Big/\left(n^s S^r\right),\ \nu_g = \tau_a \rho^a \Big/\left(n^s S^a\right),\ b_w = \mu_l \Big/\left(k^l_r k\right),\ b_g = \mu_a \Big/\left(k^a_r k\right).$$

Equations (25)–(27) represent the viscoelastic wave equations of triphase partially saturated soil. The advantages of the proposed viscoelastic dynamic model can describe the effect of both the flow-independent and flow-dependent viscosities on the soil dynamic behavior. The flow-independent viscosity is represented by the shear and dilatant constants λ_v and μ_v in Equations (25)–(27). According to Equation (1), the soil skeleton viscosity can be represented by the relaxation time t_s. Correspondingly, the fluid viscosity is characterized by the coefficients b_w and b_g in Equations (26) and (27). Apparently, the flow-dependent viscosity can finally be characterized by the intrinsic permeability k.

3. Wavefield Solution for Bulk and Rayleigh Waves

Considering the decomposition law of potential function, the displacement vector of each phase is written as

$$\boldsymbol{u}^{ph} = \nabla\varphi^{ph} + \nabla\times\boldsymbol{\psi}^{ph},\ ph = s,\ w,\ g \tag{28}$$

Substituting Equation (28) into Equations (25)–(27), the following equations are yielded as

$$\left.\begin{array}{c}\left(C_{11}+2\mu_e\right)\nabla^2\varphi^s + C_{12}\nabla^2\varphi^w + C_{13}\nabla^2\varphi^g + \left(C_{14}+2\mu_v\right)\nabla^2\dot{\varphi}^s = \rho\ddot{\varphi}^s + \rho^l\ddot{\varphi}^w + \rho^a\ddot{\varphi}^g \\ C_{21}\nabla^2\varphi^s + C_{22}\nabla^2\varphi^w + C_{23}\nabla^2\varphi^g + C_{24}\nabla^2\dot{\varphi}^s = \rho^l\ddot{\varphi}^s + v_w\ddot{\varphi}^w + b_w\dot{\varphi}^w \\ C_{31}\nabla^2\varphi^s + C_{32}\nabla^2\varphi^w + C_{33}\nabla^2\varphi^g + C_{34}\nabla^2\dot{\varphi}^s = \rho^a\ddot{\varphi}^s + v_g\ddot{\varphi}^g + b_g\dot{\varphi}^g\end{array}\right\} \tag{29}$$

$$\left.\begin{array}{c}\rho\ddot{\boldsymbol{\psi}}^s + \rho^l\ddot{\boldsymbol{\psi}}^w + \rho^a\ddot{\boldsymbol{\psi}}^g = \mu_e\nabla^2\boldsymbol{\psi}^s + \mu_v\nabla^2\dot{\boldsymbol{\psi}}^s \\ \rho^l\ddot{\boldsymbol{\psi}}^s + v_w\ddot{\boldsymbol{\psi}}^w + b_w\dot{\boldsymbol{\psi}}^w = 0 \\ \rho^a\ddot{\boldsymbol{\psi}}^s + v_g\ddot{\boldsymbol{\psi}}^g + b_g\dot{\boldsymbol{\psi}}^g = 0\end{array}\right\} \tag{30}$$

3.1. Bulk Waves

For the bulk wave propagation in the triphase unsaturated soil, the displacement potentials of solid, liquid, and air phases in Equations (29) and (30) can be expressed as

$$\varphi^{ph} = A^{ph}\exp\left[\mathrm{i}\left(\omega t - k_p\boldsymbol{r}\right)\right] \tag{31}$$

$$\boldsymbol{\psi}^{ph} = \boldsymbol{B}^{ph}\exp\left[\mathrm{i}\left(\omega t - k_s\boldsymbol{r}\right)\right] \tag{32}$$

where $\omega = 2\pi f$, and $\mathrm{i} = \sqrt{-1}$.

The following formulas are obtained by combining Equations (29)–(32), as

$$\begin{pmatrix}\rho\omega^2 - \left[\left(C_{11}+2\mu_e\right)+\mathrm{i}\,\omega\left(C_{14}+2\mu_v\right)\right]k_p^2 & \rho^l\omega^2 - C_{12}k_p^2 & \rho^a\omega^2 - C_{13}k_p^2 \\ \rho^l\omega^2 - \left(C_{21}+C_{24}\,\mathrm{i}\,\omega\right)k_p^2 & v_w\omega^2 - b_w\,\mathrm{i}\,\omega - C_{22}k_p^2 & -C_{23}k_p^2 \\ \rho^a\omega^2 - \left(C_{31}+C_{34}\,\mathrm{i}\,\omega\right)k_p^2 & -C_{32}k_p^2 & v_g\omega^2 - b_g\,\mathrm{i}\,\omega - C_{33}k_p^2\end{pmatrix}\begin{pmatrix}A^s\\A^w\\A^g\end{pmatrix} = \begin{pmatrix}0\\0\\0\end{pmatrix} \tag{33}$$

$$\begin{pmatrix}\rho\omega^2 - \left(\mu_e+\mu_v\,\mathrm{i}\,\omega\right)k_s^2 & \rho^l\omega^2 & \rho^a\omega^2 \\ \rho^l\omega^2 & v_w\omega^2 - b_w\,\mathrm{i}\,\omega & 0 \\ \rho^a\omega^2 & 0 & v_g\omega^2 - b_g\,\mathrm{i}\,\omega\end{pmatrix}\begin{pmatrix}\boldsymbol{B}^s\\\boldsymbol{B}^w\\\boldsymbol{B}^g\end{pmatrix} = \begin{pmatrix}0\\0\\0\end{pmatrix} \tag{34}$$

Finally, the characteristic equations for bulk waves in triphase unsaturated viscoelastic soil are derived from Equations (33) and (34) as

$$\begin{vmatrix}L_{11} & L_{12} & L_{13}\\ L_{21} & L_{22} & L_{23}\\ L_{31} & L_{32} & L_{33}\end{vmatrix} = 0 \tag{35}$$

$$\begin{vmatrix}J_{11} & J_{12} & J_{13}\\ J_{21} & J_{22} & J_{23}\\ J_{31} & J_{32} & J_{33}\end{vmatrix} = 0 \tag{36}$$

with

$$L_{11} = \rho\omega^2 - \left[\left(C_{11}+2\mu_e\right)+\mathrm{i}\,\omega\left(C_{14}+2\mu_v\right)\right]k_p^2,\ L_{12} = \rho^l\omega^2 - C_{12}k_p^2,\ L_{13} = \rho^a\omega^2 - C_{13}k_p^2,$$
$$L_{21} = \rho^l\omega^2 - \left(C_{21}+C_{24}\,\mathrm{i}\,\omega\right)k_p^2,\ L_{22} = v_w\omega^2 - b_w\,\mathrm{i}\,\omega - C_{22}k_p^2,\ L_{23} = -C_{23}k_p^2,$$

$$L_{31}=\rho^a\omega^2-\left(C_{31}+C_{34}\,\mathrm{i}\,\omega\right)k_p^2,\ L_{32}=-C_{32}k_p^2,\ L_{33}=v_g\omega^2-b_g\,\mathrm{i}\,\omega-C_{33}k_p^2,$$
$$J_{11}=\rho\omega^2-\left(\mu_e+\mu_v\,\mathrm{i}\,\omega\right)k_s^2,\ J_{12}=\rho^l\omega^2,\ J_{13}=\rho^a\omega^2,\ J_{21}=\rho^l\omega^2,\ J_{22}=v_w\omega^2-b_w\,\mathrm{i}\,\omega$$
$$,\ J_{23}=J_{32}=0,\ J_{31}=\rho^a\omega^2,J_{33}=v_g\omega^2-b_g\,\mathrm{i}\,\omega.$$

For the complex wavenumber of the longitudinal wave, Equation (35) can be solved into three meaningful solutions. This means that three kinds of longitudinal waves exist in unsaturated soil. The three longitudinal waves are usually signed as P_1, P_2, and P_3 waves, and the speed of the P_1 wave is the fastest, the P_2 wave is in the middle, whereas the P_3 wave is the slowest. Similarly, Equation (36) can be solved to one meaningful solution for the complex wavenumber of the transverse wave. That is, only one kind of transverse wave exists in unsaturated soil, usually labeled as S wave. Additionally, the following formulas can be yielded from Equations (33)–(36) as

$$p^{ws}=\frac{A^w}{A^s}=\frac{L_{11}L_{23}-L_{21}L_{13}}{L_{22}L_{13}-L_{12}L_{23}},\ p^{gs}=\frac{A^g}{A^s}=\frac{L_{11}L_{22}-L_{21}L_{12}}{L_{23}L_{12}-L_{13}L_{22}} \tag{37}$$

$$s^{ws}=\frac{\boldsymbol{B}^w}{\boldsymbol{B}^s}=-\frac{J_{21}}{J_{22}},\ s^{gs}=\frac{\boldsymbol{B}^g}{\boldsymbol{B}^s}=-\frac{J_{31}}{J_{33}} \tag{38}$$

Generally, the wave speed and attenuation coefficient of bulk waves are defined as

$$v_{p1}=\frac{\omega}{\mathrm{Re}\left(k_{p1}\right)},\ v_{p2}=\frac{\omega}{\mathrm{Re}\left(k_{p2}\right)},\ v_{p3}=\frac{\omega}{\mathrm{Re}\left(k_{p3}\right)},\ v_s=\frac{\omega}{\mathrm{Re}\left(k_s\right)} \tag{39}$$

$$\delta_{p1}=\mathrm{Im}\left(k_{p1}\right),\ \delta_{p2}=\mathrm{Im}\left(k_{p2}\right),\ \delta_{p3}=\mathrm{Im}\left(k_{p3}\right),\ \delta_s=\mathrm{Im}\left(k_s\right) \tag{40}$$

3.2. Rayleigh Wave

As portrayed in Figure 2, the Rayleigh wave is generated by superimposing the longitudinal and transverse waves at the soil boundary $z = 0$. Accordingly, the displacement potential in Equations (29) and (30) for the Rayleigh wave can be further rewritten as

$$\left.\begin{aligned}\varphi^s&=\left[A_{(1)}^s\,\mathrm{e}^{-\mathrm{i}\gamma_1 z}+A_{(2)}^s\,\mathrm{e}^{-\mathrm{i}\gamma_2 z}+A_{(3)}^s\,\mathrm{e}^{-\mathrm{i}\gamma_3 z}\right]\mathrm{e}^{\mathrm{i}(\omega t-k_R x)}\\ \varphi^w&=\left[p_{(1)}^{ws}A_{(1)}^s\,\mathrm{e}^{-\mathrm{i}\gamma_1 z}+p_{(2)}^{ws}A_{(2)}^s\,\mathrm{e}^{-\mathrm{i}\gamma_2 z}+p_{(3)}^{ws}A_{(3)}^s\,\mathrm{e}^{-\mathrm{i}\gamma_3 z}\right]\mathrm{e}^{\mathrm{i}(\omega t-k_R x)}\\ \varphi^g&=\left[p_{(1)}^{gs}A_{(1)}^s\,\mathrm{e}^{-\mathrm{i}\gamma_1 z}+p_{(2)}^{gs}A_{(2)}^s\,\mathrm{e}^{-\mathrm{i}\gamma_2 z}+p_{(3)}^{gs}A_{(3)}^s\,\mathrm{e}^{-\mathrm{i}\gamma_3 z}\right]\mathrm{e}^{\mathrm{i}(\omega t-k_R x)}\end{aligned}\right\} \tag{41}$$

$$\left.\begin{aligned}\boldsymbol{\psi}^s&=\boldsymbol{B}^s\,\mathrm{e}^{-\mathrm{i}\gamma_4 z}\,\mathrm{e}^{\mathrm{i}(\omega t-k_R x)}\\ \boldsymbol{\psi}^w&=s^{ws}\boldsymbol{B}^s\,\mathrm{e}^{-\mathrm{i}\gamma_4 z}\,\mathrm{e}^{\mathrm{i}(\omega t-k_R x)}\\ \boldsymbol{\psi}^g&=s^{gs}\boldsymbol{B}^s\,\mathrm{e}^{-\mathrm{i}\gamma_4 z}\,\mathrm{e}^{\mathrm{i}(\omega t-k_R x)}\end{aligned}\right\} \tag{42}$$

where

$$\gamma_1=\sqrt{k_{p1}^2-k_R^2},\ \gamma_2=\sqrt{k_{p2}^2-k_R^2},\ \gamma_3=\sqrt{k_{p3}^2-k_R^2},\ \gamma_4=\sqrt{k_s^2-k_R^2} \tag{43}$$

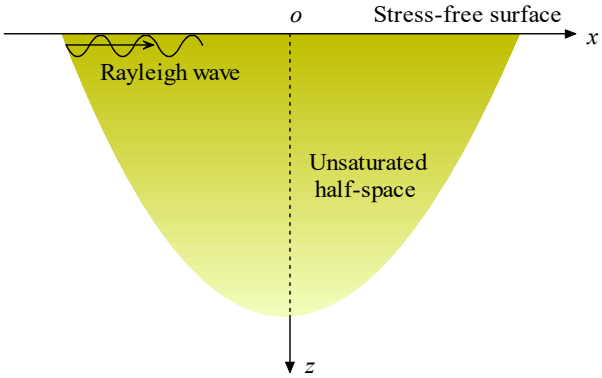

Figure 2. The semi-infinite system of Rayleigh wave propagation.

As discussed earlier, the Rayleigh wave in unsaturated soil is a kind of superimposed wave at the soil boundary. In this work, considering the stress-free boundary, the stresses (σ_{zz} and σ_{xz}) and fluid pressures (p_l and p_a) disappear at the soil boundary. Accordingly, the following formulas can be obtained as

$$\sigma_{zz}=\left(C_{11}+C_{14}\frac{\partial}{\partial t}\right)\left(\frac{\partial u_x^s}{\partial x}+\frac{\partial u_z^s}{\partial z}\right)+2\left(\mu_e+\mu_v\frac{\partial}{\partial t}\right)\frac{\partial u_z^s}{\partial z}+C_{12}\left(\frac{\partial u_x^w}{\partial x}+\frac{\partial u_z^w}{\partial z}\right)+C_{13}\left(\frac{\partial u_x^g}{\partial x}+\frac{\partial u_z^g}{\partial z}\right)=0 \tag{44}$$

$$\sigma_{xz}=\left(\mu_e+\mu_v\frac{\partial}{\partial t}\right)\left(\frac{\partial u_x^s}{\partial z}+\frac{\partial u_z^s}{\partial x}\right)=0 \tag{45}$$

$$p_l=-\left(C_{21}+C_{24}\frac{\partial}{\partial t}\right)\left(\frac{\partial u_x^s}{\partial x}+\frac{\partial u_z^s}{\partial z}\right)-C_{22}\left(\frac{\partial u_x^w}{\partial x}+\frac{\partial u_z^w}{\partial z}\right)-C_{23}\left(\frac{\partial u_x^g}{\partial x}+\frac{\partial u_z^g}{\partial z}\right)=0 \tag{46}$$

$$p_a=-\left(C_{31}+C_{34}\frac{\partial}{\partial t}\right)\left(\frac{\partial u_x^s}{\partial x}+\frac{\partial u_z^s}{\partial z}\right)-C_{32}\left(\frac{\partial u_x^w}{\partial x}+\frac{\partial u_z^w}{\partial z}\right)-C_{33}\left(\frac{\partial u_x^g}{\partial x}+\frac{\partial u_z^g}{\partial z}\right)=0 \tag{47}$$

Substituting Equations (41) and (42) into Equations (44)–(47) and making algebraic operations, the following formula can be derived as

$$\begin{pmatrix}\Re_{11} & \Re_{12} & \Re_{13} & \Re_{14}\\ \Re_{21} & \Re_{22} & \Re_{23} & \Re_{24}\\ \Re_{31} & \Re_{32} & \Re_{33} & \Re_{34}\\ \Re_{41} & \Re_{42} & \Re_{43} & \Re_{44}\end{pmatrix}\begin{pmatrix}A_{(1)}^s\\ A_{(2)}^s\\ A_{(3)}^s\\ \boldsymbol{B}^s\end{pmatrix}=\begin{pmatrix}0\\0\\0\\0\end{pmatrix} \tag{48}$$

with

$$\Re_{11}=2\left(\mu_e+\mu_v\,\mathrm{i}\,\omega\right)\gamma_1^2+\left[C_{11}+C_{14}\,\mathrm{i}\,\omega+C_{12}p_{(1)}^{ws}+C_{13}p_{(1)}^{gs}\right]k_{p1}^2,$$

$$\Re_{12}=2\left(\mu_e+\mu_v\,\mathrm{i}\,\omega\right)\gamma_2^2+\left[C_{11}+C_{14}\,\mathrm{i}\,\omega+C_{12}p_{(2)}^{ws}+C_{13}p_{(2)}^{gs}\right]k_{p2}^2,$$

$$\Re_{13}=2\left(\mu_e+\mu_v\,\mathrm{i}\,\omega\right)\gamma_3^2+\left[C_{11}+C_{14}\,\mathrm{i}\,\omega+C_{12}p_{(3)}^{ws}+C_{13}p_{(3)}^{gs}\right]k_{p3}^2,\ \Re_{14}=2\left(\mu_e+\mu_v\,\mathrm{i}\,\omega\right)k_R\gamma_4,$$

$$\Re_{21}=2\left(\mu_e+\mu_v\,\mathrm{i}\,\omega\right)\gamma_1k_R,\ \Re_{22}=2\left(\mu_e+\mu_v\,\mathrm{i}\,\omega\right)\gamma_2k_R,\ \Re_{23}=2\left(\mu_e+\mu_v\,\mathrm{i}\,\omega\right)\gamma_3k_R,$$

$$\Re_{24}=\left(\mu_e+\mu_v\,\mathrm{i}\,\omega\right)\left(k_R^2-\gamma_4^2\right),\ \Re_{31}=\left[C_{21}+C_{24}\,\mathrm{i}\,\omega+C_{22}p_{(1)}^{ws}+C_{23}p_{(1)}^{gs}\right]k_{p1}^2,$$

$$\Re_{32}=\left[C_{21}+C_{24}\,\mathrm{i}\,\omega+C_{22}p_{(2)}^{ws}+C_{23}p_{(2)}^{gs}\right]k_{p2}^{2},\ \Re_{33}=\left[C_{21}+C_{24}\,\mathrm{i}\,\omega+C_{22}p_{(3)}^{ws}+C_{23}p_{(3)}^{gs}\right]k_{p3}^{2},$$
$$\Re_{41}=\left[C_{31}+C_{34}\,\mathrm{i}\,\omega+C_{32}p_{(1)}^{ws}+C_{33}p_{(1)}^{gs}\right]k_{p1}^{2},\ \Re_{42}=\left[C_{31}+C_{34}\,\mathrm{i}\,\omega+C_{32}p_{(2)}^{ws}+C_{33}p_{(2)}^{gs}\right]k_{p2}^{2},$$
$$\Re_{43}=\left[C_{31}+C_{34}\,\mathrm{i}\,\omega+C_{32}p_{(3)}^{ws}+C_{33}p_{(3)}^{gs}\right]k_{p3}^{2},\ \Re_{34}=\Re_{44}=0$$

Finally, the characteristic equation of the Rayleigh wave is derived from Equation (48) as

$$\begin{vmatrix}\Re_{11} & \Re_{12} & \Re_{13} & \Re_{14}\\ \Re_{21} & \Re_{22} & \Re_{23} & \Re_{24}\\ \Re_{31} & \Re_{32} & \Re_{33} & \Re_{34}\\ \Re_{41} & \Re_{42} & \Re_{43} & \Re_{44}\end{vmatrix}=0 \tag{49}$$

By solving Equation (49), the wave speed (v_R) and attenuation coefficient (δ_R) of Rayleigh are solved as

$$v_R=\omega/\mathrm{Re}(k_R),\ \delta_R=\mathrm{Im}(k_R) \tag{50}$$

4. Numerical Examples and Parametric Analysis

This section will utilize numerical calculation and parametric analysis to analyze the dependence of physical parameters for the soil on the motion behaviors (mainly for the speed and attenuation) of bulk and Rayleigh waves. The value of the soil parameter in the following calculation examples refers to Table 1 [2] unless otherwise specified.

Table 1. Physical parameters of unsaturated soil.

Parameter	Value	Parameter	Value	Parameter	Value
n^s	0.4	K_s	36 GPa	λ_e	120 MPa
S^r	0.6	K_l	2.2 GPa	μ_e	120 MPa
S_{res}	0.05	K_a	0.1 MPa	μ^l	0.001 Pa·s
ρ^s	2650 kg·m^{-3}	χ	0.0001	μ^a	1.8 × 10^{-5} Pa·s
ρ^l	1000 kg·m^{-3}	m	0.5	τ_l	1.0
ρ^a	1.3 kg·m^{-3}	d	2.0	τ_a	1.0
k	1.0 × 10^{-11} m^2	f	100 Hz		

When t_s is set to zero, the unsaturated porous viscoelastic model developed in this work can be reduced to the traditional, unsaturated poroelastic model. Thus, the results obtained in this work can be validated through comparing them with the results developed in previous work. The comparison results for the wave velocities of P_1, S, and Rayleigh waves between this work and the work developed by Yang [2] are presented in Figure 3a, which shows that the analytical solutions obtained by this work and Yang [2] have a good agreement. Additionally, Murphy [37] carried out acoustic measurements of partial gas saturation in tight sandstones employing a pulse transmission technique, obtaining the wave speeds of P_1 and S waves. Accordingly, this work introduces the physical parameters of tight sandstones [37] and calculates the corresponding wave speeds of P_1 and S waves. The calculated results from this work are compared with the experimental measurement results observed by Murphy [37], as portrayed in Figure 3b. The comparison results in Figure 3 have good consistency both quantitatively and qualitatively.

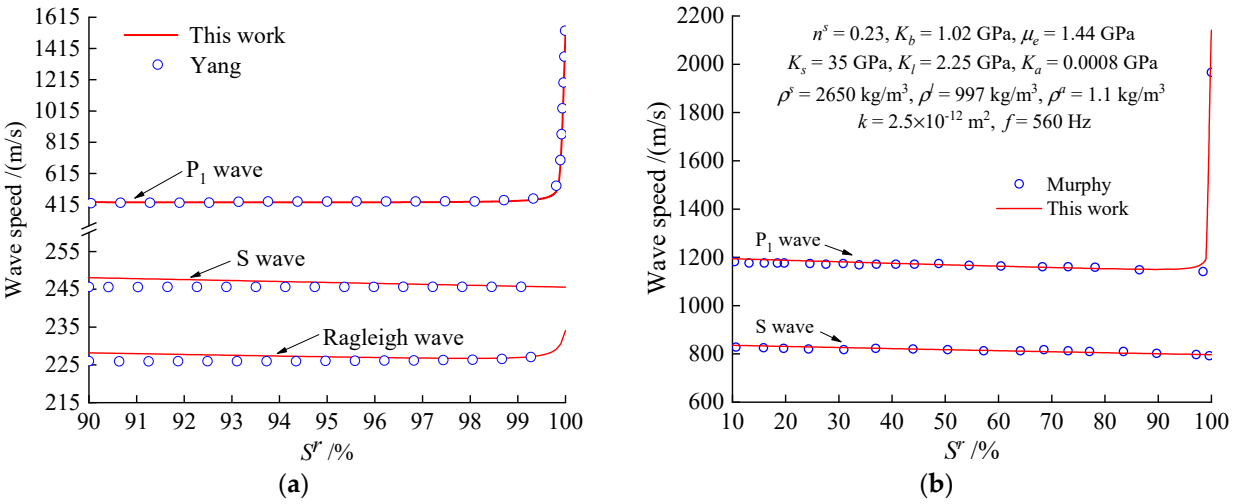

Figure 3. Comparisons of the wave speed between this study and the works done by Yang [2] and Murphy [37]. (**a**) Comparison with Yang (2005). (**b**) Comparison with Murphy (1984).

Figures 4–6 depict the variations for v_{p1}, v_s, v_R, δ_{p1}, δ_s, and δ_R under various values of S^r and t_s, where S^r ranges from 10% to 100% and t_s is taken to be 0 s, 0.5×10^{-3} s, and 1.0×10^{-3} s, respectively. As depicted in Figures 4–6, v_{p1} is the largest, followed by v_s, and then v_R. In contrast, the order of attenuation coefficients runs entirely counter to the order of wave speed. As shown in Figures 4a, 5a and 6a, v_{p1}, v_s, and v_R decrease obviously with the increase of S^r when the foundation soil is partially saturated. Although, there is a sudden sharp increase in v_{p1} and v_R but not in v_s when the foundation soil reaches complete saturation state. At the same time, as clarified in Figures 4b, 5b and 6b, the variations of δ_{p1}, δ_s, and δ_R with S^r run diametrically counter to that of v_{p1}, v_s, and v_R with S^r. On the other side, the effects of t_s on v_{p1}, v_s, v_R, δ_{p1}, δ_s, and δ_R are conspicuous from the variations in Figures 4–6. For P_1, S, and Rayleigh waves, the curves reveal that v_{p1}, v_s, v_R, δ_{p1}, δ_s, and δ_R enlarge with the increase of t_s value. In practical engineering, P_1, S, and Rayleigh waves are the main application object, whereas P_2 and P_3 waves (not shown graphically in this work) are challenging to observe in engineering practice due to their slow speed and fast attenuation. Therefore, for the works of wave propagation in unsaturated or saturated foundation soil, it is essential to account for the effect of flow-independent viscosity from the solid skeleton. Additionally, the soil–water characteristic curve (SWCC) is depicted in Figure 7 (ϕ represents the matric suction), illustrating that the increase of S^r will reduce the matric suction ϕ of soil. When soil is completely saturated (S^r = 100%), ϕ will decrease to 0. Undoubtedly, the effect of ϕ and S^r on the motion behaviors (speed and attenuation) of bulk and Rayleigh waves is opposite.

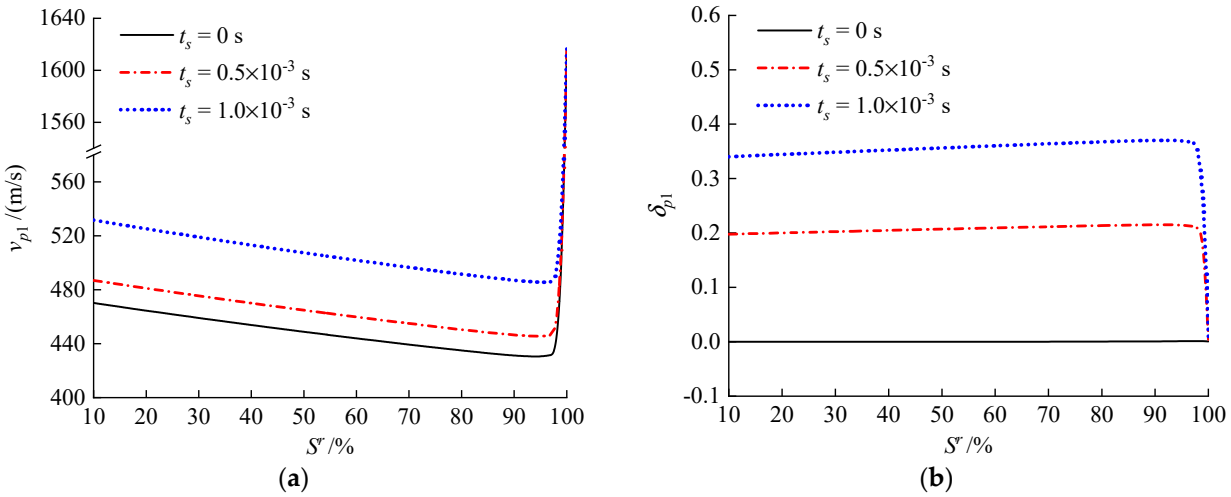

Figure 4. P1 wave propagation for different saturations and relaxation times. (**a**) Wave speed. (**b**) Attenuation coefficient.

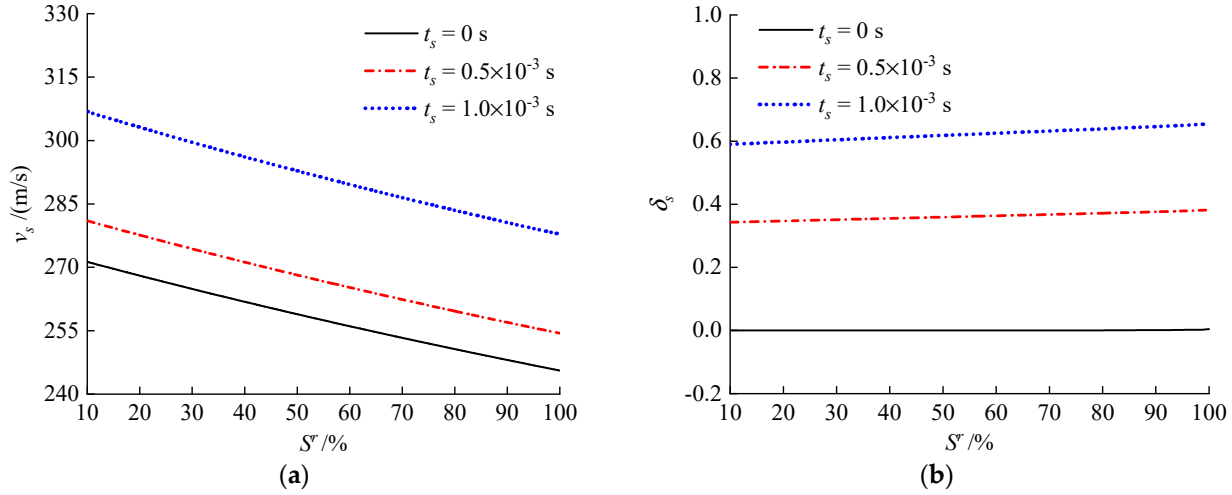

Figure 5. S wave propagation for different saturations and relaxation times. (**a**) Wave speed. (**b**) Attenuation coefficient.

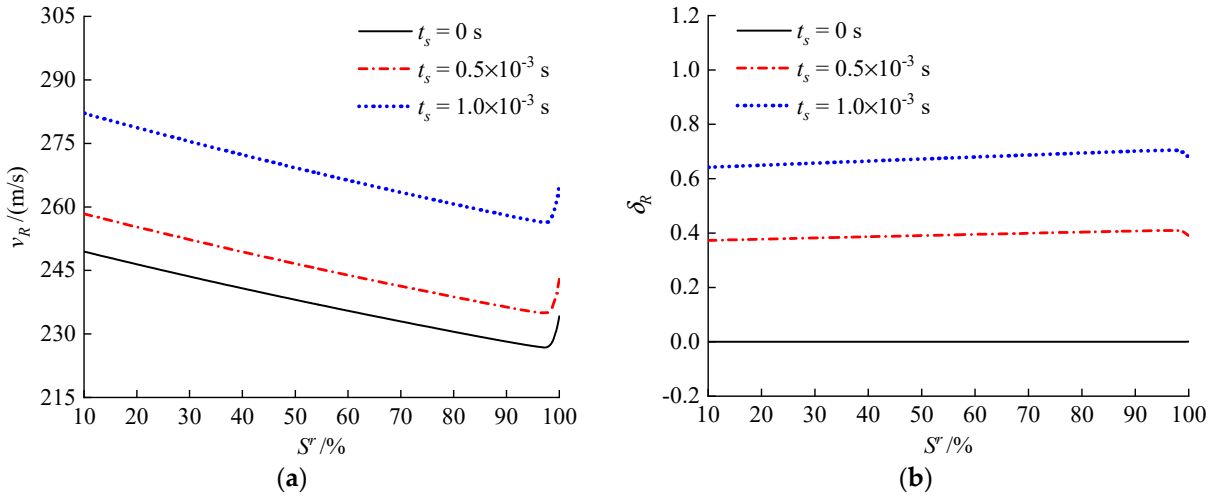

Figure 6. Rayleigh wave propagation for different saturations and relaxation times. (**a**) Wave speed. (**b**) Attenuation coefficient.

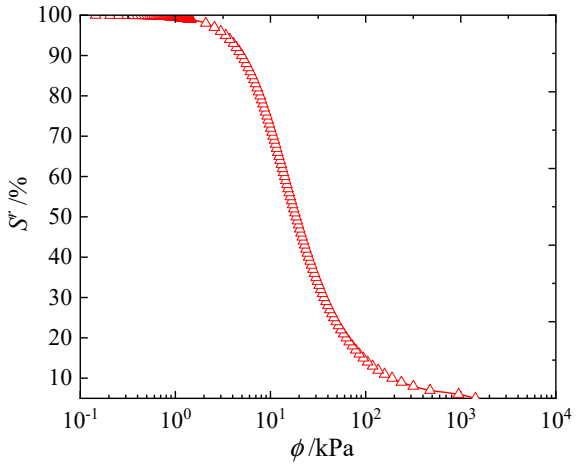

Figure 7. Soil–water characteristic curve (SWCC).

The dependency of v_{p1}, v_s, v_R, δ_{p1}, δ_s, and δ_R on t_s and f are depicted in Figures 8–10, therein f ranges from 0.01 Hz to 150 Hz, t_s is taken to be 0 s, 0.5 × 10⁻³ s, and 1.0 × 10⁻³ s, respectively, and the value of other physical parameters refers to Table 1. It can be captured from Figures 8–10 that each wave presents positive relativity between both the wave speeds and attenuation coefficients and the frequency. In contrast, this positive relativity will be hidden when the soil skeleton viscosity is not considered. This is a vital issue worthy of attention in practical engineering applications. Meanwhile, Figures 8–10 show that the increase of v_{p1}, v_s, v_R, δ_{p1}, δ_s, and δ_R will accompany the enlargement of t_s.

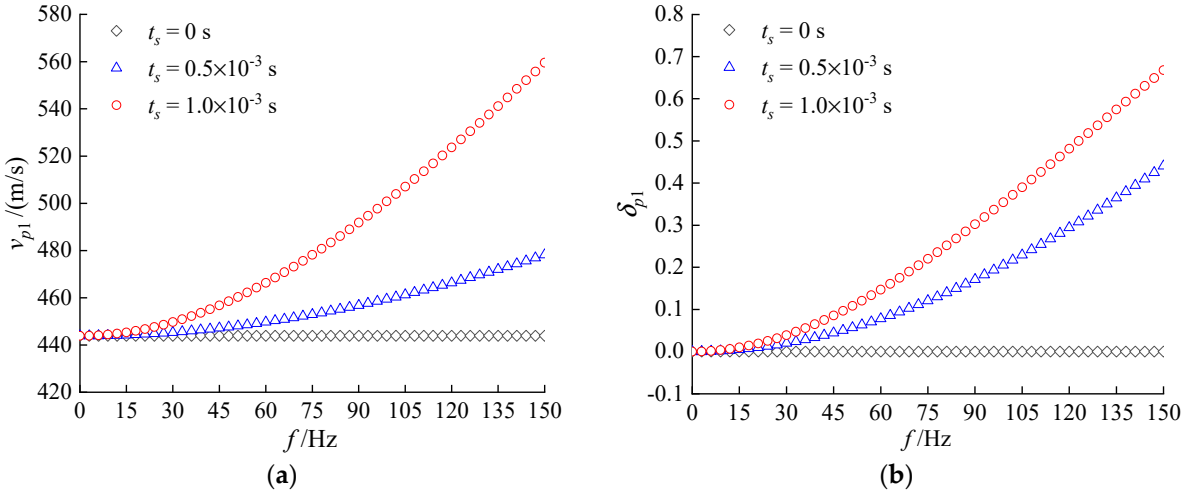

Figure 8. P_1 wave propagation for different frequencies and relaxation times. (**a**) Wave speed. (**b**) Attenuation coefficient.

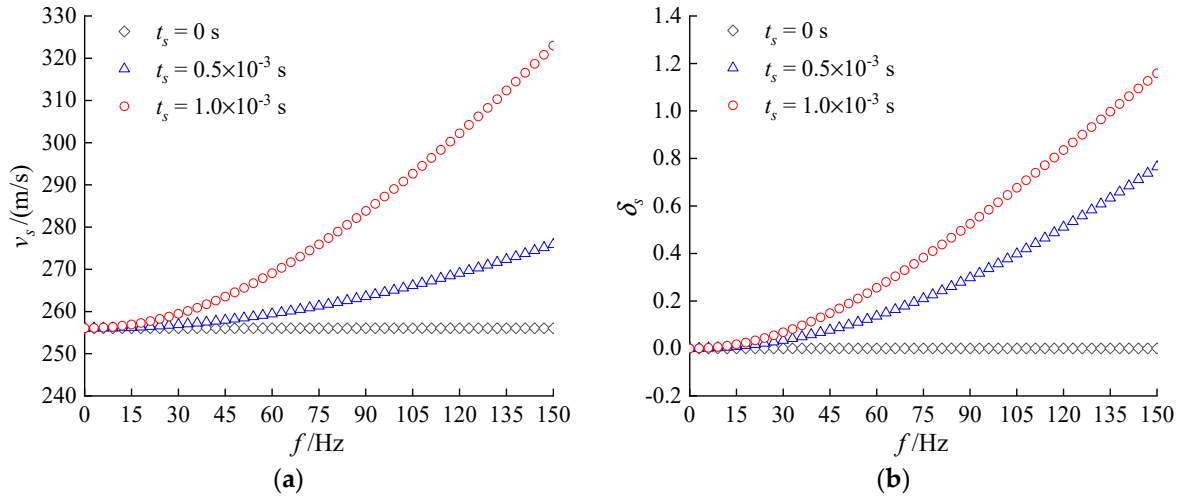

Figure 9. S wave propagation for different frequencies and relaxation times. (**a**) Wave speed. (**b**) Attenuation coefficient.

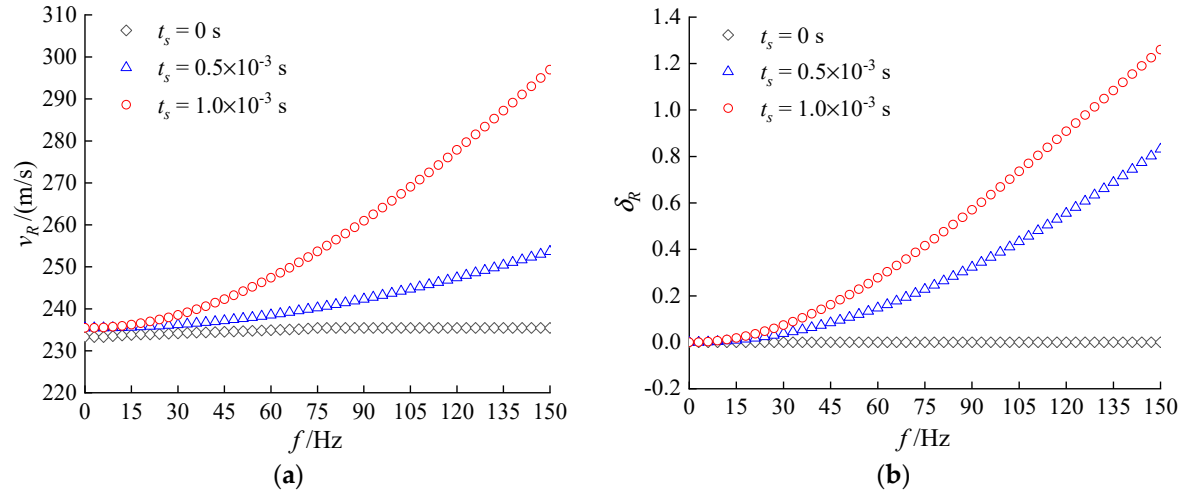

Figure 10. Rayleigh wave propagation for different frequencies and relaxation times. (**a**) Wave speed. (**b**) Attenuation coefficient.

As mentioned in Equations (25)–(27), the flow-dependent viscosities from pore-liquid and pore-air are characterized by the parameters b_w and b_g in Equations (26) and (27) and finally represented by the intrinsic permeability k. For comparison, Figures 11–13 demonstrate the effects of k and t_s on v_{p1}, v_s, v_R, δ_{p1}, δ_s, and δ_R. In this example, the value range of k is 10^{-12}~10^{-7} m^2, while t_s ranges from 0 × 10^{-3} s to 2.0 × 10^{-3} s. It can be seen from Figures 11a, 12a and 13a that v_{p1}, v_s, and v_R remain unchanged when k is in the range of 10^{-12}~10^{-9} m^2 but increase gradually with the enlargement of k in the high permeability zone (i.e., k = 10^{-9} m^2~10^{-7} m^2). For δ_{p1}, δ_s, and δ_R, the variation trends in Figures 11b, 12b and 13b display an approximately normal distribution in the entire permeability range. Furthermore, as above-mentioned discussion, the increase of t_s will make the dependences of v_{p1}, v_s, v_R, δ_{p1}, δ_s, and δ_R on k move upward along the positive direction of the vertical axis. Apparently, through comparison, it can be seen that compared to the fluid viscosity, the soil skeleton viscosity has a more prominent contribution to the motion behaviors (speed and attenuation) of elastic waves and is more significant for practical engineering applications.

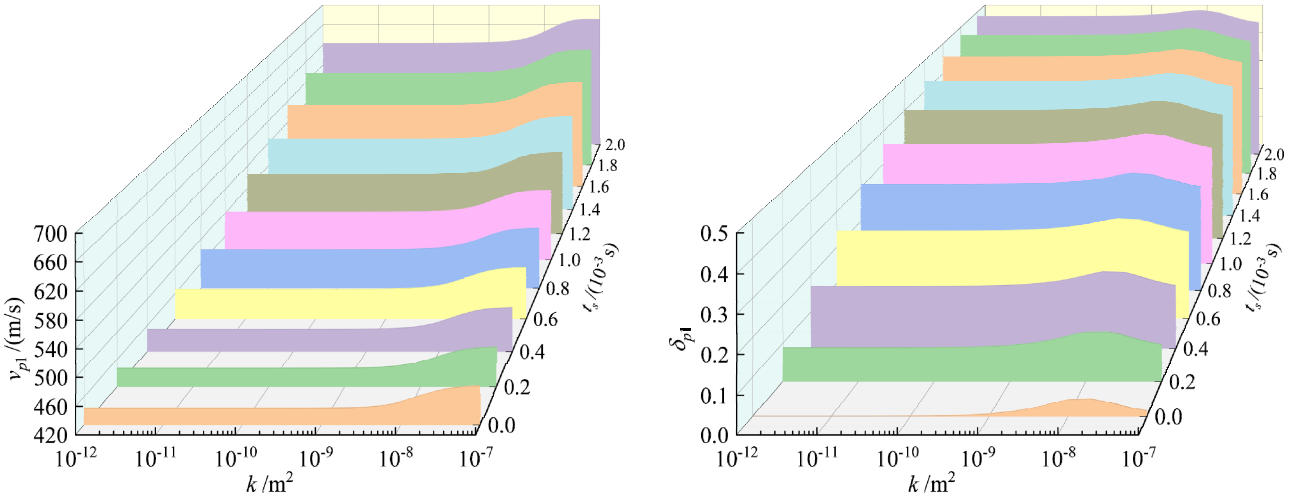

Figure 11. P_1 wave propagation for different intrinsic permeabilities and relaxation times. (**a**) Wave speed. (**b**) Attenuation coefficient.

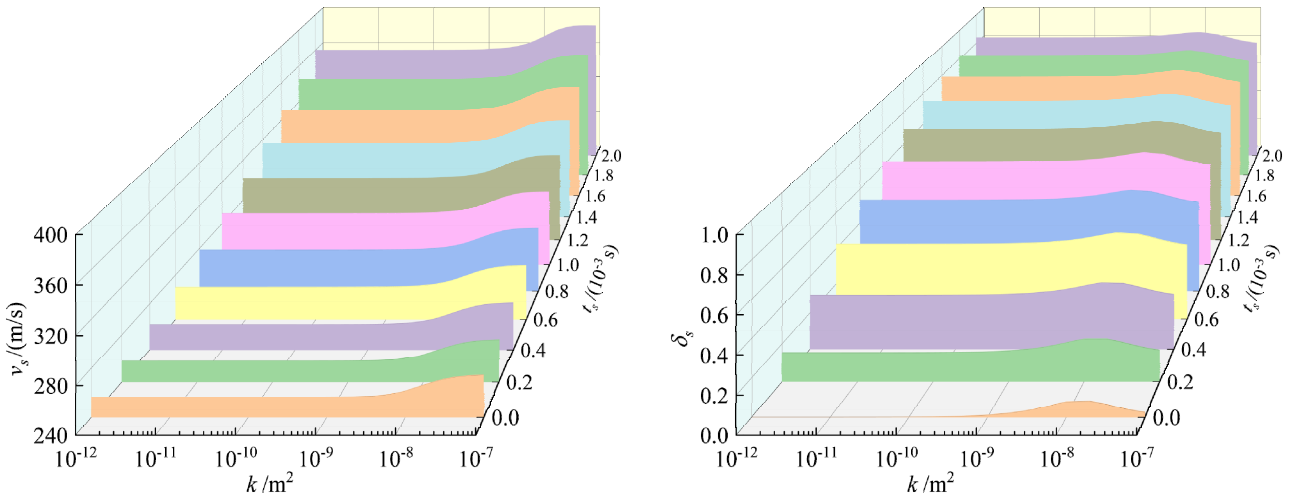

Figure 12. S wave propagation for different intrinsic permeabilities and relaxation times. (**a**) Wave speed. (**b**) Attenuation coefficient.

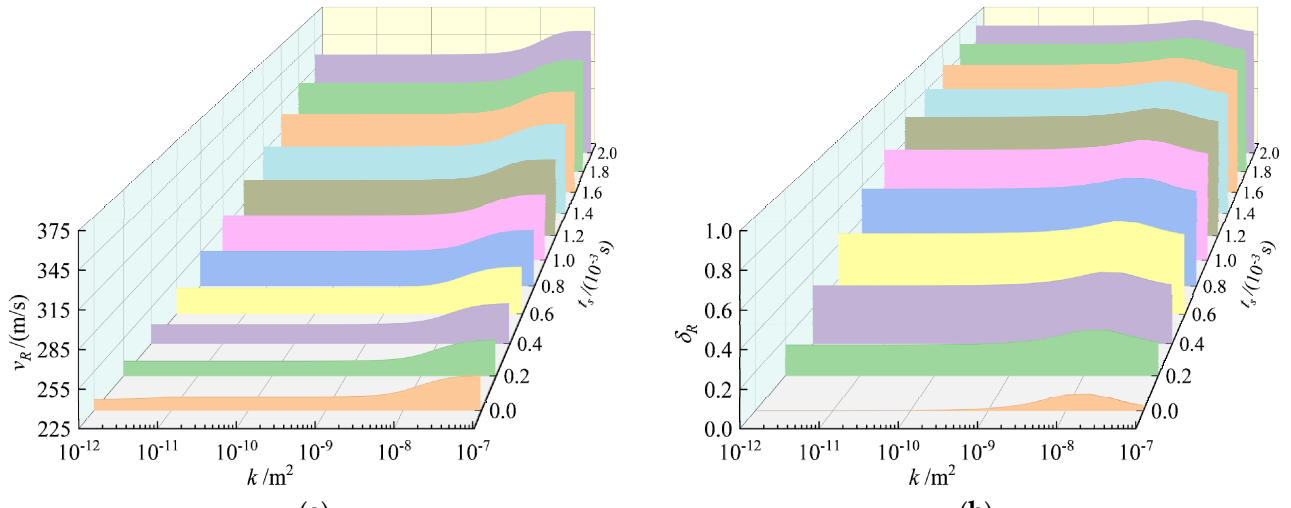

Figure 13. Rayleigh wave propagation for different intrinsic permeabilities and relaxation times. (**a**) Wave speed. (**b**) Attenuation coefficient.

The increase in the relaxation time will influence the interaction between the microscopic particles of the material, and thus will change the wave speed and attenuation coefficient of the bulk and Rayleigh waves. The effect of saturation on the propagation behavior of bulk and Rayleigh waves can be attributed to the increase of saturation. The volume of liquid in soil pores increases, and thus the flow-dependent viscosity increases. It leads to the reduction of the wave velocity of elastic waves and the acceleration of attenuation. However, when the soil tends to be fully saturated, the mutual coupling of the liquid and gas phase disappears, resulting in the disappearance of the capillary effect and matric suction of the soil, so that the wave speeds of P_1 and Rayleigh waves suddenly increase and the attenuation coefficients suddenly decrease. The soil intrinsic permeability represents a quantitative property of porous material, depending solely on the pore structure of porous material. The larger the intrinsic permeability, the smaller the effect of flow viscosity on the propagation of bulk and Rayleigh waves, which will have a greater effect on its wave speed and attenuation coefficient.

5. Conclusions

In this article, considering the influence of both the flow-independent and flow-dependent viscosities for soils on the elastic wave propagation, a modified viscoelastic dynamic model of the three-phase partially saturated soil is established to investigate the motion behaviors of bulk and Rayleigh waves. The characteristics equations of bulk and Rayleigh waves have been yielded analytical in explicit form. The dependences of the motion behaviors (speed and attenuation) for various waves on the physical parameters are graphed through employing several numerical examples. The main conclusions are summarized as follows: (i) Both the wave speed and attenuation coefficient of P_1, S, and Rayleigh waves increase obviously with the flow-independent viscosity at both the partially and completely saturated states; (ii) In the high permeability zone, both the flow-independent and flow-dependent viscosities have an apparent influence on the propagation for P_1, S, and Rayleigh waves; (iii) In the low and middle permeability zone, only the flow-independent viscosity affects the propagation behavior for P_1, S, and Rayleigh waves.

Author Contributions: All authors conceived and designed the study. Conceptualization, methodology, and writing—review and editing: Q.G., H.L., and G.D.; writing—original draft preparation and visualization: Q.G. and H.L.; investigation and resources: Z.L. and Q.G.; supervision: G.D. All authors have read and agreed to the published version of the manuscript.

Funding: This research was funded by the National Natural Science Foundation of China (NSFC Grant Nos. 52078128, 51878160).

Institutional Review Board Statement: Not applicable.

Informed Consent Statement: Not applicable.

Data Availability Statement: Data are contained within the article.

Conflicts of Interest: The authors declare no conflict of interest.

Nomenclature

The nomenclature of symbols in this paper

Roman Symbols

A^{ph}	scalar potential amplitudes of ph phase
$\boldsymbol{B}^{ph}$	vector potential amplitude of ph phase
c^{e}_{ij}	isotropic elastic coefficient matrix of soil skeleton
c^{s}_{ij}	isotropic viscoelastic coefficient matrix of soil skeleton
d	fitting parameters of unsaturated soil

f	conventional frequency
i	imaginary unit
k	intrinsic permeability of unsaturated soil
k_R	complex wavenumber of Rayleigh wave
k_p	complex wavenumber of longitudinal wave
k_s	complex wavenumber of transverse wave
k_r^a	relative permeability of gas phase
k_r^l	relative permeability of liquid phase
K_b	bulk modulus of soil skeleton
K_a	bulk modulus of gas phase
K_l	bulk modulus of liquid phase
K_s	compression modulus of soil particles
m	fitting parameters of unsaturated soil
n^s	porosity of unsaturated soil
p	averaged pore pressure
p_a	gas pressure
p_l	liquid pressure
$\boldsymbol{r}$	position vector
S^a	gas saturation
S^r	liquid saturation
S_e	effective liquid saturation
S_{res}	liquid saturation at residual state
t_s	relaxation time
u_i^a	displacement component of gas phase
u_i^l	displacement component of liquid phase
u_i^s	displacement component of solid phase
u_i^g	relative displacement of gas phase
u_i^w	relative displacement of liquid phase
v_{p1}	wave speed of P_1 wave
v_{p2}	wave speed of P_2 wave
v_{p3}	wave speed of P_3 wave
v_s	wave speed of S wave.

Greek Symbols

γ_1	wavenumber component of P_1 wave in z-direction
γ_2	wavenumber component of P_2 wave in z-direction
γ_3	wavenumber component of P_3 wave in z-direction
γ_4	wavenumber component of S wave in z-direction
δ_{ij}	Kronecker delta
δ_{p1}	attenuation coefficient of P_1 wave
δ_{p2}	attenuation coefficient of P_2 wave
δ_{p3}	attenuation coefficient of P_3 wave
δ_s	attenuation coefficient of S wave
ε_v	volumetric strain of soil skeleton
ε_{ij}	strain tensor under general state
ε_{ij}^p	strain tensor under pore pressure
$\lambda_e,\ \mu_e$	elastic constant of soil
$\lambda_v,\ \mu_v$	viscosity constants of soil
μ_a	dynamic viscosity of gas phases
μ_l	dynamic viscosity of liquid phase
ρ^a	mass density of gas phase
ρ^l	mass density of liquid phase
ρ^s	mass density of solid phase
$\overline{\rho}^a$	apparent density of gas phase
$\overline{\rho}^l$	apparent density of liquid phase
$\overline{\rho}^s$	apparent density of solid phase
σ_{ij}	total stress

σ'_{ij}	effective stress tensor of unsaturated soil
τ_a	tortuosity of gas phase
τ_l	tortuosity of liquid phase
φ^{ph}	scalar potential of ph phase
$\boldsymbol{\psi}^{ph}$	vector potentials of ph phase
χ	fitting parameters of unsaturated soil
ω	angular frequency.

References

1. Berryman, J.G. Confirmation of Biot's theory. *Appl. Phys. Lett.* **1980**, *37*, 382–384.
2. Yang, J. Rayleigh surface waves in an idealised partially saturated soil. *Géotechnique* **2005**, *55*, 409–414.
3. Biot, M.A. Theory of propagation of elastic waves in a fluid-saturated porous solid. I. Low-frequency range. *J. Acoust. Soc. Am.* **1956**, *28*, 168–178.
4. Biot, M.A. Theory of propagation of elastic waves in a fluid-saturated porous solid. II. Higher frequency range. *J. Acoust. Soc. Am.* **1956**, *28*, 179–191.
5. Bowen, R.M. Incompressible porous media models by use of the theory of mixtures. *Int. J. of Eng. Sci.* **1980**, *18*, 1129–1148.
6. Jones, J.P. Rayleigh waves in a porous, elastic, saturated solid. *J. Acoust. Soc. Am.* **1961**, *33*, 959–962.
7. Plona, T.J. Observation of a second bulk compressional wave in a porous medium at ultrasonic frequencies. *Appl. Phys. Lett.* **1980**, *36*, 259–261.
8. Berryman, J.G.; Thigpen, L.; Chin, R.C. Bulk elastic wave propagation in partially saturated porous solids. *J. Acoust. Soc. Am.* **1988**, *84*, 360–373.
9. Berryman, J.G. Fluid effects on shear waves in finely layered porous media. *Geophysics* **2005**, *70*, N1–N15.
10. Zhou, F.; Ma, Q. Propagation of Rayleigh waves in fluid-saturated non-homogeneous soils with the graded solid skeleton distribution. *Int. J. Numer. Anal. Methods Geomech.* **2016**, *40*, 1513–1530.
11. Straughan, B.; Tibullo, V.; Amendola, A. Nonlinear acceleration wave propagation in the DKM theory. *Mech. Res. Commun.* **2020**, *104*, 103482.
12. Rohan, E.; Nguyen, V.H.; Naili, S. Homogenization approach and Floquet-Bloch theory for wave analysis in fluid-saturated porous media with mesoscopic heterogeneities. *Appl. Math. Model.* **2021**, *91*, 1–23.
13. Tung, D.X. Surface waves in nonlocal transversely isotropic liquid-saturated porous solid. *Arch. Appl. Mech.* **2021**, *91*, 2881–2892.
14. Wang, B.; Zhang, X.; Sun, B. Propagation prediction of body waves in fluid-saturated soils with flow-independent viscosity. *Symmetry* **2022**, *14*, 408.
15. Fattah, M.Y.; Abbas, S.F.; Karim, H.H. A model for coupled dynamic elastic-plastic analysis of soils. *J. GeoEngineering* **2012**, *7*, 43–50.
16. Fattah, M.Y.; Al Mosawi, M.J.; Al Ameri, A.F. Dynamic response of saturated soil-foundation system acted upon by vibration. *J. Earthq. Eng.* **2017**, *21*, 1158–1188.
17. Alzabeebee, S. Dynamic response and design of a skirted strip foundation subjected to vertical vibration. *Geomech. Eng.* **2020**, *20*, 345–358.
18. Alzabeebee, S. Numerical analysis of the interference of two active machine foundations. *Geotech. Geol. Eng.* **2020**, *38*, 5043–5059.
19. Lo, W.C. Propagation and attenuation of Rayleigh waves in a semi-infinite unsaturated poroelastic medium. *Adv. Water Resour.* **2008**, *31*, 1399–1410.
20. Lo, W.C.; Yeh, C.L.; Lee, J.W. Effect of viscous cross coupling between two immiscible fluids on elastic wave propagation and attenuation in unsaturated porous media. *Adv. Water Resour.* **2015**, *83*, 207–222.
21. Liu, H.; Zhou, F.; Wang, L.; Zhang, R. Propagation of Rayleigh waves in unsaturated porothermoelastic media. *Int. J. Numer. Anal. Met.* **2020**, *44*, 1656–1675.
22. Liu, H.; Dai, G.; Zhou, F.; Mu, Z. Propagation behavior of homogeneous plane-P1-wave at the interface between a thermoelastic solid medium and an unsaturated porothermoelastic medium. *Eur. Phys. J. Plus* **2021**, *136*, 1163.
23. Liu, H.; Dai, G.; Zhou, F.; Cao, X. A mixture theory analysis for reflection phenomenon of homogeneous plane-P1-wave at the boundary of unsaturated porothermoelastic media. *Geophys. J. Int.* **2022**, *228*, 1237–1259.
24. Bardet, J.P. A Viscoelastic Model for the Dynamic Behavior of Saturated Poroelastic Soils. *J. Appl. Mech.* **1992**, *59*, 128–135.
25. Xie, K.; Liu, G.; Shi, Z. Dynamic response of partially sealed circular tunnel in viscoelastic saturated soil. *Soil Dyn. Earthq. Eng.* **2004**, *24*, 1003–1011.
26. Chen, W.; Wang, D.; Mou, Y.; Zhao, K.; Chen, G. Effect of flow-independent viscosity on the propagation of Rayleigh wave in porous media. *Soil Dyn. Earthq. Eng.* **2021**, *142*, 106564.
27. Cheng, Z.; Leong, E.C. Finite element simulations of wave propagation in soils using a Viscoelastic model. *Soil Dyn. Earthq. Eng.* **2016**, *88*, 207–214.

28. Sills, G.C.; Wheeler, S.J.; Thomas, S.D.; Gardner, T.N. Behaviour of offshore soils containing gas bubbles. *Géotechnique* **1991**, *41*, 227–241.
29. Michaels, P. In situ determination of soil stiffness and damping. *J. Geotech. Geoenviron. Eng.* **1998**, *124*, 709–719.
30. Militano, G.; Rajapakse, R. Dynamic response of a pile in a multi-layered soil to transient torsional and axial loading. *Géotechnique* **1999**, *49*, 91–109.
31. Zhou. F.; Liu, H.; Li, S. Propagation of thermoelastic waves in unsaturated porothermoelastic media. *J. Therm. Stress.* **2019**, *42*, 1256–1271.
32. Bishop, A.W.; Blight, G. Some aspects of effective stress in saturated and partly saturated soils. *Géotechnique* **1963**, *13*, 177–197.
33. Zhang, M.; Wang, X.; Yang, G.; Xie, L. Solution of dynamic Green's function for unsaturated soil under internal excitation. *Soil Dyn. Earthq. Eng.* **2014**, *64*, 63–84.
34. Van Genuchten, M.T. A closed-form equation for predicting the hydraulic conductivity of unsaturated soils. *Soil Sci. Soc. Am. J.* **1980**, *44*, 892–898.
35. Capeillère, J.; Mesgouez, A.; Lefeuve-Mesgouez, G. Axisymmetric wave propagation in multilayered poroelastic grounds due to a transient acoustic point source. *Soil Dyn. Earthq. Eng.* **2013**, *52*, 70–76.
36. Mualem, Y. A new model for predicting the hydraulic conductivity of unsaturated porous media. *Water Resour. Res.* **1976**, *12*, 513–522.
37. Murphy, W.F. Acoustic measures of partial gas saturation in tight sandstones. *J. Geophys. Res.* **1984**, *89*, 11549–11559.